ELSEVIER

Chemical Engineering Science 59 (2004) 417–424

Chemical Engineering Science

www.elsevier.com/locate/ces

Purely viscous flow of a shear-thinning fluid between two rotating spheres

Eric Lee, June-Kuo Ming, Jyh-Ping Hsu*

Department of Chemical Engineering, National Taiwan University, Taipei, Taiwan 10617, ROC

Received 14 April 2003; received in revised form 12 September 2003; accepted 14 October 2003

Abstract

The steady-state flow of a non-Newtonian fluid in the space between two concentric spheres, both may rotate at constant angular velocities, is analyzed using a pseudo-spectral method based on Chebyshev polynomials. We focus our attention specifically upon the effect of shear thinning on the behavior of the system under investigation. The Carreau fluid, which is characterized by a power-law exponent n and a time constant λ, is selected as the representative case. We find that if the spheres are rotating at different directions, only one single vortex can exist if n is small. This is in contrast to the corresponding Newtonian fluid case, where two vortexes of opposite orientations are observed. This is an interesting discovery in the fundamental non-Newtonian fluid mechanics, which differs drastically from the conventional Newtonian fluid mechanics. Also, if the outer sphere is fixed, the torque required to rotate the inner sphere increases almost linearly with the increase of n. This information is of practical importance for the design of agitated polymeric reactors, for instance, among other potential engineering applications.

Keywords: Shear thinning; Concentric rotating spheres; Pseudo-spectral method

1. Introduction

The fast development of polymeric materials and associated polymer processing operations in the past several decades has evoked significant research endeavors on the study of non-Newtonian fluid mechanics. Crucial achievements were documented and analyzed extensively by Bird et al. (1977). In the conventional fluid mechanics, the viscosity of fluid is assumed to be a constant, which does not vary with the velocity field, or equivalently, the velocity gradient (shear rate). However, the shear-thinning phenomenon, the decrease of viscosity as shear rate increases, is frequently observed in non-Newtonian fluids such as polymer melts or solutions (Tucker III, 1989). As a result, a thorough understanding of its impact on the related variables is essential before any reliable engineering design involving such a fluid is possible.

Following rigorous derivations similar to those in the Newtonian case, a set of governing equations can be established, in general, for further analysis in the field of non-Newtonian fluid flows. The basic difference is the replacement of the Navier–Stokes equation by the more fundamental Cauchy momentum equation, as discussed by Bird et al. (1977). Because the resultant governing equations are highly non-linear even under creeping flow situation, the solution-finding procedure is much more complicated and difficult than that in the corresponding Newtonian case. Numerical approach is normally required for cases of practical interests. For example, in the calculation of the power required to operate a polymerization reactor, Ide and White (1974) modeled the flow patterns around agitators using an idealized and simplified configuration, which assumed that the reacting fluid is confined between two concentric rotating spheres; the elasticity of the fluid was taken into account. Unfortunately, the shear-thinning effect was neglected in their analysis, which was actually crucial in a typical engineering set-up like theirs. The analysis of Ide and White was extended recently by Lee et al. (2002b) to take this important effect into account, where the shear-thinning effect on both the elasticity and the viscosity were investigated. This is so far the most general treatment of the topic. The CEF model (Bird et al., 1977) adopted by the authors was also used by

* Corresponding author. Tel.: +886-2-2363-7448; fax: +886-2-2362-3040.

E-mail address: jphsu@ccms.ntu.edu.tw (J.-P. Hsu).

0009-2509/$ - see front matter © 2003 Elsevier Ltd. All rights reserved.
doi:10.1016/j.ces.2003.10.007

Bar-Yoseph and Kryzhanovski (1996) in a study of the flow of a non-isothermal polymeric fluid under other conditions.

In practice, there are many flow situations where the elasticity of a non-Newtonian fluid is either completely absent or negligible, whereas purely viscous behavior with shear-thinning effect on viscosity alone is significant. It is still non-Newtonian in the sense that the viscosity is not a constant, but a function of shear rate. To treat topics of this nature, we select here the flow of a shear thinning yet purely viscous fluid contained between two concentric rotating spheres as a representative case to study. This selection is partly based on the fact that such a system is actually a classic problem in fluid mechanics in the corresponding Newtonian fluid case (Pearson, 1967; Greenspan, 1968, 1975; Pedlosky, 1969). Previous results include both experimental observations and theoretical analyses; the latter includes both analytical and numerical studies. Another crucial motivation to focus on the sphere-in-sphere geometry is its potential applications in other fields. In colloidal science (Nakabayashi and Tsuchida, 1995; Nakabayashi et al., 1995; Endo and Kousaka, 1996), for example, it is often adopted to study the boundary effect on electrophoresis. The electrophoresis of a spherical entity in a spherical cavity for the case of a Newtonian fluid was analyzed by Chu et al. (2001) and Lee et al. (2002a), and that for the case of a non-Newtonian fluid was investigated by Lee et al. (2003). In this study, the non-Newtonian rheological behavior of a fluid is simulated by a Carreau model (Bird et al., 1977), which incorporates both the Newtonian and the well-known power-law fluids as its limiting cases. This is especially ideal for the present study because it makes the direct comparison with the available Newtonian results straightforward.

Because of the complicated nature of the problem under consideration, adopting a numerical approach is inevitable. Various numerical methods of finite difference type were used in the past to treat related systems (Dennis and Quartapelle, 1984; Schultz et al., 1991). Here, a pseudo-spectral method (Gottlieb et al., 1984) based on Chebyshev polynomials is chosen to solve the governing partial differential equations. This method is relatively simple to apply, and is known to have the merits such as higher order of convergence than normally accomplished by the finite difference method, and the convergent properties are independent of boundary conditions (Karageorghis, 1991). Also, it has been proven to be a very powerful and efficient tool in recent studies regarding the electrokinetic phenomena of colloids (Lee et al., 1998, 1999, 2000, 2001).

2. Theory

Let us consider the steady-state behaviors of the system illustrated in Fig. 1, where a sphere of radius R_1 is placed at the center of a sphere of radius R_2. The space between these spheres is filled with a Carreau fluid. The inner and the outer spheres are rotating independently with constant angular velocities ω_1 and ω_2, respectively, around the Z-axis. The spherical coordinates (r, θ, ϕ) are adopted with its origin located at the center of the inner sphere. Note that because the problem under consideration is ϕ-symmetric, it is of two-dimensional nature, and considering only one of the quadrants of the plane represented by $\phi =$ constant is sufficient. The governing equations for the flow of a shear-thinning fluid confined in the space between two concentric spheres can be expressed as

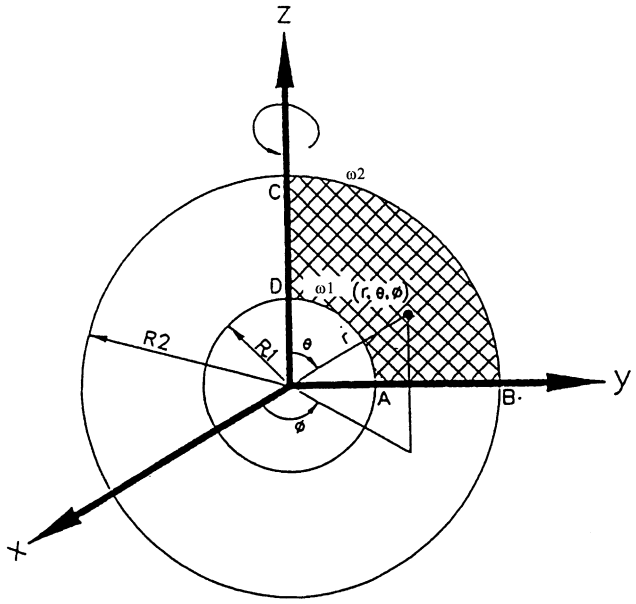

Fig. 1. The problem under consideration where a sphere of radius R_1 is placed at the center of a spherical cavity of radius R_2, the former rotates with constant angular velocity ω_1 and the latter rotates with constant velocity ω_2 around the Z-axis. The space between the sphere and the cavity is filled with a Carreau fluid. Spherical coordinates (r, θ, ϕ) are adopted with its origin located at the center of the cavity.

$$\rho \underline{V} \cdot \nabla \underline{V} = -\nabla P + \eta \nabla^2 \underline{V} + (\nabla \eta) \cdot \underline{\underline{\dot{\gamma}}}, \tag{1}$$

$$\nabla \cdot \underline{V} = 0. \tag{2}$$

In these expressions, ρ and η are, respectively, the density and the viscosity of fluid, P is the pressure, ∇ is the gradient operator, $\underline{V}$ is fluid velocity, and $\underline{\underline{\dot{\gamma}}}$ is the shear rate tensor defined by

$$\underline{\underline{\dot{\gamma}}} = \tfrac{1}{2} (\nabla \underline{V} + \nabla \underline{V}^{\mathrm{T}}). \tag{3}$$

The superscript T denotes matrix transpose. Eq. (1) is a generalized Navier–Stokes equation, which is based on the Cauchy momentum equation. The last term on its right-hand side takes the shear-thinning effect of fluid viscosity into account, which is absent in the classic Navier–Stokes equation for a Newtonian fluid. Eq. (2) is the continuity equation for an incompressible fluid, which is the case considered here. For the present case, the Carreau model below is adopted to

describe the shear-thinning behavior of fluid:

$$\eta = \eta_0[1 + (\lambda\dot{\gamma})^2]^{(n-1)/2}, \tag{4}$$

where η_0 is the limiting value of η as $\dot{\gamma} \to 0$, λ is a time constant pertinent to the fluid, $\dot{\gamma}$ is the magnitude of $\underline{\underline{\dot{\gamma}}}$, and n is a shear-thinning index. Note that if either $\lambda = 0$ or $n = 1$, η becomes a constant and we have a Newtonian fluid, and when $\lambda\dot{\gamma} \gg 1$, Eq. (4) describes a power-law fluid. Also, if η is a constant, Eq. (1) reduces to

$$\rho\underline{V} \cdot \nabla\underline{V} = -\nabla P + \eta\nabla^2\underline{V}, \tag{5}$$

which is the classic Navier–Stokes equation for a Newtonian fluid. Here, the effect of gravitational force is neglected.

For convenience, dimensionless variables are used in subsequent discussions. To this end, we define $r = R_s r^*$, $t = t_s t^*$, $v = R_s v^*/t_s$, $P = \eta_0 P^*/t_s$, $\underline{\underline{\dot{\gamma}}} = \underline{\underline{\dot{\gamma}}}^*/t_s$, $\lambda = t_s\lambda^*$, and $\eta = \eta_0\eta^*$, and $\omega_s = \max\{\omega_1, \omega_2\}$, where a symbol with an asterisk denotes a dimensionless quantity. In terms of these symbols, Eqs. (1), (2), and (4) become

$$Re(\underline{V}^* \cdot \nabla^*\underline{V}^*) = -\nabla^* P^* + \eta^*\nabla^{*2}\underline{V}^* + (\nabla^*\eta^*) \cdot \underline{\underline{\dot{\gamma}}}^*, \tag{6}$$

$$\nabla^* \cdot \underline{V}^* = 0, \tag{7}$$

$$\eta^* = [1 + (\lambda^*\dot{\gamma}^*)^2]^{(n-1)/2}, \tag{8}$$

where $Re = \rho R_2^2\omega_s/\eta_0$ is the Reynolds number.

To simply subsequent mathematical treatments, a stream function representation for the flow field is adopted. Note that by adopting this representation, the continuity equation is satisfied automatically. In terms of the dimensionless stream function ψ^*, the velocity components in the r- and θ-directions, v_r^* and v_θ^*, can be expressed as

$$v_r^* = \frac{1}{r^{*2}\sin\theta}\frac{\partial\psi^*}{\partial\theta}, \tag{9}$$

$$v_\theta^* = -\frac{1}{r^*\sin\theta}\frac{\partial\psi^*}{\partial r^*}, \tag{10}$$

ψ^* and the original stream function ψ are related by $\psi = (R_2^3\omega_s)\psi^*$. Similarly, the vorticity function $\Omega = v_\phi r\sin\theta$ is introduced, and we define the corresponding dimensionless vorticity function as $\Omega = \Omega^* R_2^2\omega_s$. The dimensionless velocity component in the ϕ-direction, v_ϕ^*, can be expressed as

$$v_\phi^* = \frac{\Omega^*}{r^*\sin\theta}. \tag{11}$$

In terms of dimensionless symbols, the momentum equation, or the generalized Navier–Stokes equation becomes

$$\eta^* D^{*2}\Omega^* + \frac{Re}{r^{*2}\sin\theta}\left[\frac{\partial\psi^*}{\partial r^*}\frac{\partial\Omega^*}{\partial\theta} - \frac{\partial\psi^*}{\partial\theta}\frac{\partial\Omega^*}{\partial r^*}\right] = -r^*\sin\theta\left(\frac{\partial\eta^*}{\partial r^*}\dot{\gamma}_{r\phi}^* + \frac{1}{r^*}\frac{\partial\eta^*}{\partial\theta}\dot{\gamma}_{\theta\phi}^*\right), \tag{12}$$

$$\eta^* D^{*4}\psi^* + Re\left[\frac{2\Omega^*}{r^{*3}\sin^2\theta}\left(\frac{\partial\Omega^*}{\partial\theta}\sin\theta - \frac{\partial\Omega^*}{\partial r^*}r^*\cos\theta\right) + \frac{1}{r^{*2}\sin\theta}\left(\frac{\partial\psi^*}{\partial r^*}\frac{\partial(D^{*2}\psi^*)}{\partial\theta} - \frac{\partial\psi^*}{\partial\theta}\frac{\partial(D^{*2}\psi^*)}{\partial r^*}\right) + \frac{2(D^{*2}\psi^*)}{r^{*3}\sin^2\theta}\left(\frac{\partial\psi^*}{\partial\theta}\sin\theta - \frac{\partial\psi^*}{\partial r^*}r^*\cos\theta\right)\right] = -\sin\theta\left[\frac{\partial\eta^*}{\partial\theta} \times (\nabla^{*2}\underline{v}^*)_r^* - \frac{\partial\eta^*}{\partial r^*} \times (r^* \times (\nabla^{*2}\underline{v}^*)_\theta) + \frac{\partial}{\partial\theta}(\nabla^*\eta^* \cdot \underline{\underline{\dot{\gamma}}}^*)_r - \frac{\partial}{\partial r^*}(r^* \times (\nabla^*\eta^* \cdot \underline{\underline{\dot{\gamma}}}^*)_\theta)\right]. \tag{13}$$

In these expressions

$$D^{*2} = \frac{\partial^2}{\partial r^{*2}} + \frac{1}{r^{*2}}\frac{\partial^2}{\partial\theta^2} - \frac{\cot\theta}{r^{*2}}\frac{\partial}{\partial\theta} \tag{14}$$

and $D^{*4} = D^{*2}(D^{*2})$. Note that because the present problem is axi-symmetric, the dependent variables in Eqs. (12) and (13) are functions of r^* and θ only.

The conventional no-slip boundary conditions on the surfaces of the inner and the outer spheres are assumed, and, together with some symmetric arguments, we have the following boundary conditions:

$$\psi^* = \frac{\partial\psi^*}{\partial r} = 0 \quad \text{on surfaces AD and BC,} \tag{15}$$

$$\psi^* = \Omega^* = 0 \quad \text{on surface CD,} \tag{16}$$

$$\Omega^* = \left(\frac{\omega_1}{\omega_s}\right)\left(\frac{R_1}{R_2}\right)^2\sin^2\theta \quad \text{on surface AD,} \tag{17}$$

$$\Omega^* = \left(\frac{\omega_2}{\omega_s}\right)\sin^2\theta \quad \text{on surface BC,} \tag{18}$$

$$\psi^* = \frac{\partial\Omega^*}{\partial\theta} = 0 \quad \text{on surface AB.} \tag{19}$$

Eqs. (12) and (13) and the associated boundary conditions, Eqs. (15)–(19), constitute a well-posed problem, which is solved by a pseudo-spectral method based on Chebyshev polynomials. The numerical method is summarized briefly in the appendix.

3. Results and discussions

Intuitively, we anticipate that the major flow observable in a purely rotational system like the present one would be in the angular, or ϕ-direction. Therefore, we focus our attention to the flow field of angular velocity to start with. Fig. 2 shows the contours of the angular velocity of the primary flow for a Newtonian fluid with dimensionless rotational speeds $\omega_1 = 1.0$ and $\omega_2 = -0.5$; the minus sign indicates a clockwise rotation, i.e., the inner and outer spheres are rotating in reverse directions. The ratio of the radius of the inner sphere to that of the outer sphere is kept as 0.5 and *Re*

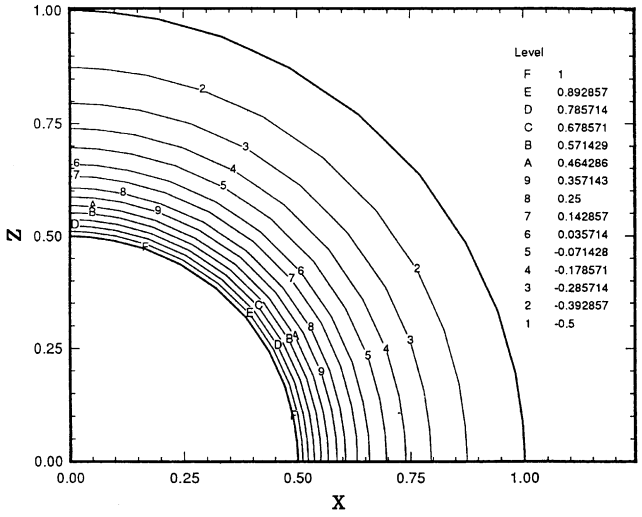

Fig. 2. Contours on the meridian plane $\phi = 0$ for the angular velocity of the primary flow for the case of Newtonian fluid with $Re = 1$, $R_1/R_2 = 0.5$, $\omega_1 = 1$, and $\omega_2 = -0.5$.

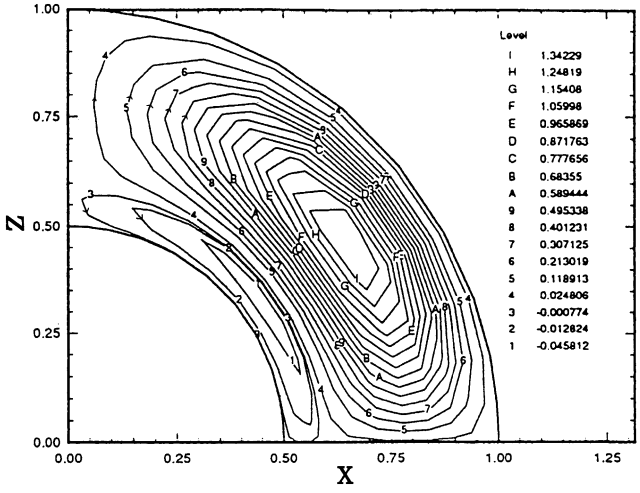

Fig. 3. Contours of stream function ($\times 10^5$) on the meridian plane $\phi = 0$ for the case of Fig. 2.

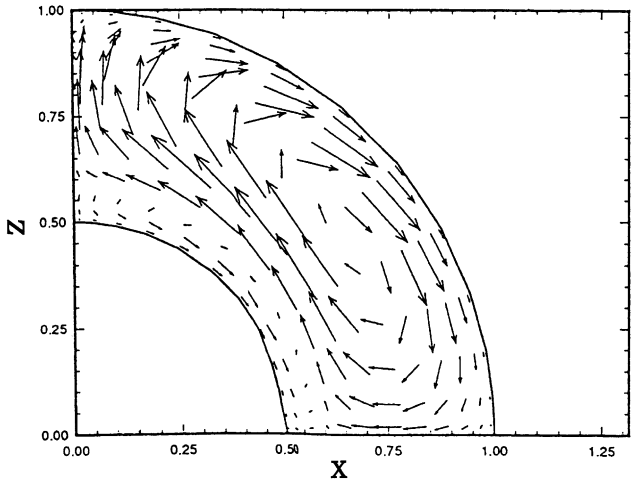

Fig. 4. Flow field on the meridian plane $\phi = 0$ for the case of Fig. 3.

is assumed the value of unity throughout this study. Because the system under consideration is ϕ-symmetric, the results on the meridian plane $\phi = 0$ are shown for illustration. The magnitude of each contour is tabulated in the upper-right region of Fig. 2. Obviously, it will decrease from 1.0 on the inner sphere all the way to -0.5 on the outer sphere. It is noticed that there is a change of sign between contours 5 and 6, which means there exists a spherical shell between these two contours where the angular velocity is essentially zero. This shell basically serves as a motionless virtual boundary separating the entire flow into two sub-regions: the inner partial spherical gap, and the outer partial spherical gap. This set the stage for the following interesting and intriguing observations.

Fig. 2 exhibits that the primary flow field behaves as a multi-layer flow, like an onion in a sense. It should be noted, however, that this is not a rigid body motion as might be expected, since the angular velocity is not a constant but position-dependent instead, as indicated by Fig. 1. As a matter of fact, two separate vortexes appear on the r–θ plane, which are inversely oriented and axi-symmetric with respect to the rotation axis, as shown in Fig. 3. These vortexes are the secondary flows superimposed on the primary flow depicted in Fig. 2, which is the direct consequence of the existence of a motionless virtual spherical shell mentioned above. The fluid within the inner partial spherical region is spun off the surface of the inner sphere, thus its orientation is counterclockwise as can be seen in Fig. 4, since the centrifugal force is at its maximum near the equator. Similarly, the fluid near the equator of the outer sphere is spun off toward the inner direction, and results in a clockwise rotating vortex, as is illustrated in Fig. 4. There is no mixing of fluids between these two vortexes, however.

When the fluid under consideration is changed to a Carreau fluid, the scenario is fundamentally different as depicted by Figs. 5–8. The geometry is the same throughout these figures, that is, the ratio of the radius of the inner sphere to that of the outer sphere is fixed at 0.5. The rotational speeds of both the inner and the outer spheres are kept exactly the same as the above Newtonian case also. Moreover, the time constant λ is fixed at unity also to eliminate its possible involvement in the shear thinning effect, as implied by Eq. (7). This choice greatly facilitates the consequent analysis since the shear thinning effect is represented solely by the magnitude of the exponent index n now. The value of n is between zero and unity, theoretically speaking, although 0.2 might be the smallest value observed in practice. The smaller the value of n, the greater the effect of shear thinning is.

Fig. 5 shows the secondary flow in the r–θ plane when n is reduced from unity to 0.7. There are still two vortexes as before, but the inner vortex is "squeezed" somehow toward the surface of the inner sphere. The region occupied initially by the inner vortex is invaded by the expansion of the

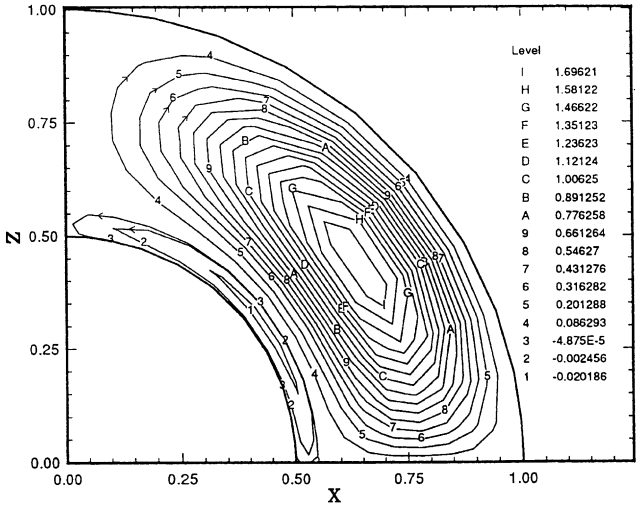

Fig. 5. Contours of stream function ($\times 10^5$) on the meridian plane $\phi = 0$ for the case of Carreau fluid with $Re = 1$, $\lambda = 1$, $n = 0.7$, $R_1/R_2 = 0.5$, $\omega_1 = 1$, and $\omega_2 = -0.5$.

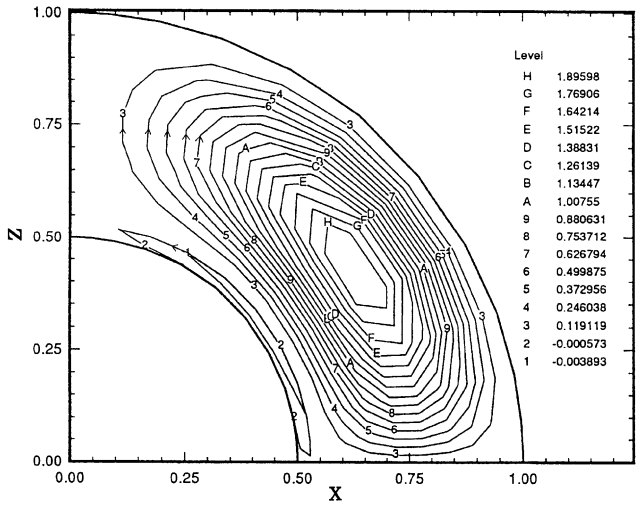

Fig. 6. Contours of stream function ($\times 10^5$) on the meridian plane $\phi = 0$ for the case of Carreau fluid with $Re = 1$, $\lambda = 1$, $n = 0.5$, $R_1/R_2 = 0.5$, $\omega_1 = 1$, and $\omega_2 = -0.5$.

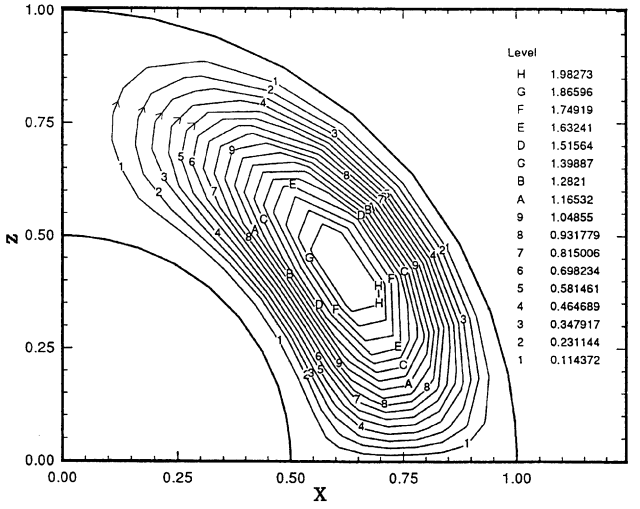

Fig. 7. Contours of stream function ($\times 10^5$) on the meridian plane $\phi = 0$ for the case of Carreau fluid with $Re = 1$, $\lambda = 1$, $n = 0.4$, $R_1/R_2 = 0.5$, $\omega_1 = 1$, and $\omega_2 = -0.5$.

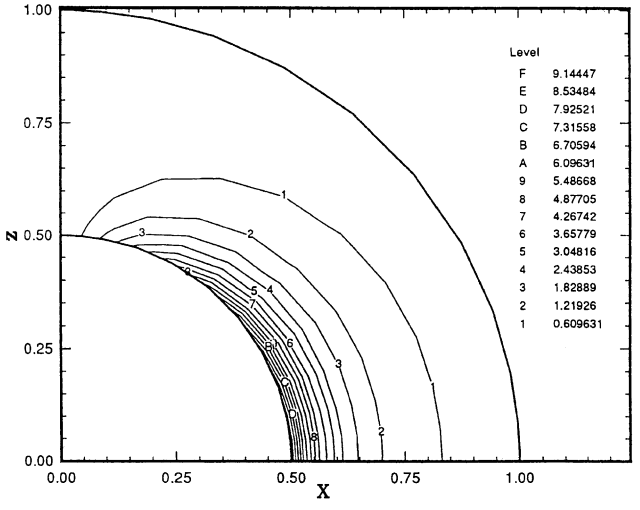

Fig. 8. Contours of shear rate $\dot{\gamma}$ on the meridian plane $\phi = 0$ for the case of Fig. 7.

outer vortex, although the orientation of each vortex does not change. The situation becomes even more dramatic as the value of n is decreased to 0.5, as shown by Fig. 6. The inner vortex is indeed very thin now. Finally, it is "swallowed" by the outer vortex completely as demonstrated by Fig. 7, where the value of n is as small as 0.4. Only one single vortex of clockwise orientation occupies the entire flow region.

The reason behind this interesting and dramatic phenomenon is the shearing-thinning effect represented by the magnitude of n. To elaborate this in detail, we use Fig. 8 to show a typical shear rate distribution ($n = 0.4$) for the above analyzed flow cases. The contour plot for shear rate is depicted with the values of each contour line tabulated in the upper right region of the figure. Obviously, shear rates near the inner rotating sphere is much higher than the region away from it. The high shear rate significantly reduces the corresponding apparent viscosity there. As a result, the momentum transfer due to the rotation of the inner sphere cannot "penetrate" deep enough into the flow region to sustain a large area of vortex (Bird et al., 2002). The smaller the value of n, the more significant this shear-thinning effect is. In the case of $n = 0.4$, the fluid near the surface of inner sphere becomes virtually inviscid, thus no vortex flow can be induced any more.

The corresponding velocity distribution of the primary flow for a Carreau fluid ($n = 0.4$) is shown in Fig. 9, and the spatial variation of viscosity is presented in Fig. 10. A comparison of this figure with Fig. 2 reveals that the flow now is

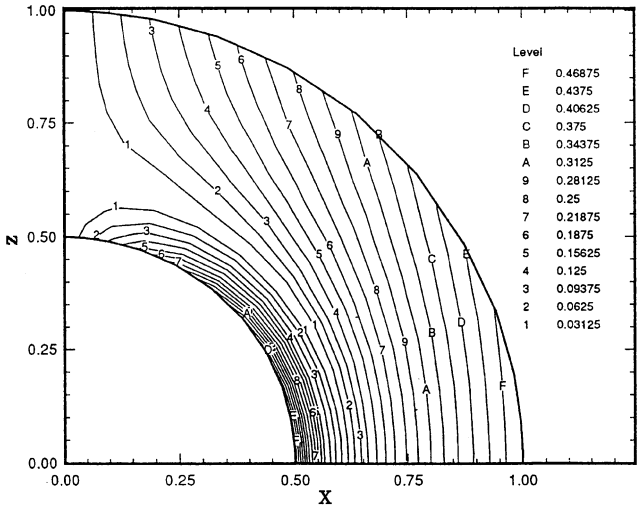

Fig. 9. Contours of angular velocity on the meridian plane $\phi = 0$ for the case of Fig. 7.

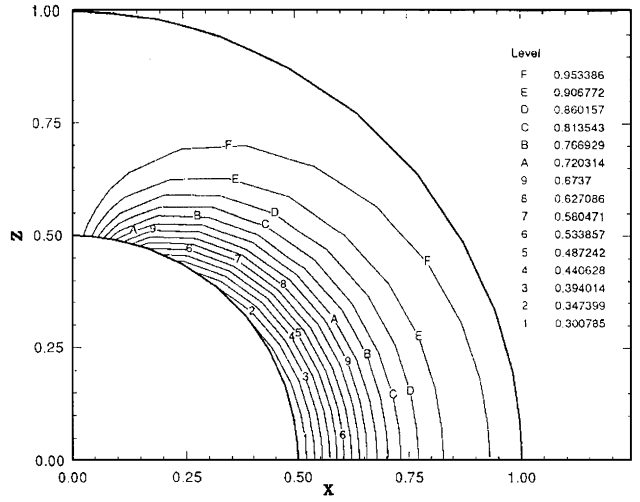

Fig. 10. Contours of viscosity on the meridian plane $\phi = 0$ for the case of Fig. 7.

no longer a concentric shells of equal-angular velocity system. In contrast to the case of a Newtonian fluid, where v_φ is a function of r only, it is now a function of both r and θ. It is interesting to note, however, that the flow region near the inner sphere is still similar to that of a spherical shell system, whereas the flow region near the outer sphere is similar to that of a co-axial cylindrical shell system. Again, this arises primarily from the shear-thinning effect. As can be seen in Fig. 10, the apparent viscosity near cavity wall is much greater than that near the inner sphere. The whole system behaves like a kind of thin fluid rotating within a concrete rigid gel. However, this phenomenon is hardly noticeable near the North Pole area, because the shear-thinning effect is quite small due to the weak centrifugal force appears there.

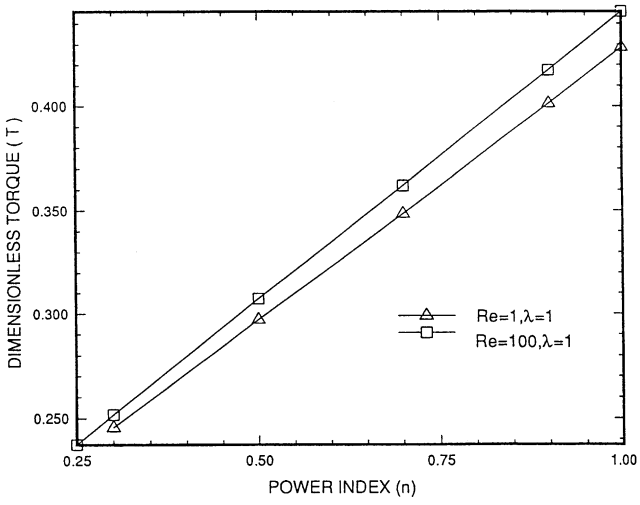

Fig. 11. Variation of scaled torque as a function of parameter n at different Re for the case $\lambda = 1$, $R_1/R_2 = 0.5$, $\omega_1 = 1$, and $\omega_2 = 0$.

Fig. 11 shows the variation of the scaled torque, using the torque for the corresponding Newtonian case as the scaling factor, as a function of n at different Reynolds numbers for the specific case where the outer sphere is kept motionless. This resembles the situation for a mixing-tank type of reactor. As can be seen from this figure, the larger the Re the greater the scaled torque, for a fixed n. Fig. 11 also reveals that the scaled torque decreases with the decrease in n, for a fixed Reynolds number. This states quantitatively the fact that the shear-thinning effect greatly reduces the torque required to rotate an agitator, modeled as a inner sphere here, within a reactor. It is also interesting to note that the scaled torque and n are almost linearly correlated. This may serve as a useful rule of thumb for the design of an agitated polymeric reactor, for instance.

4. Conclusion

Using a pseudo-spectral method based on Chebyshev polynomials, we investigate the flow of a Carreau fluid contained between two concentric spheres each rotating at a constant angular. We found that the shear-thinning effect is very significant for the system. This effect, characterized primarily by a power-law exponent n, alters the flow field dramatically compared with the corresponding conventional Newtonian fluid. The double vortexes observed at low Reynolds number when the two spheres are rotating at different directions cannot sustain as n becomes small. The inner one is swallowed entirely by the outer vortex eventually as n is as small as 0.4, for the specific case under discussion. This is elaborated as the direct consequence of the shear-thinning effect.

Furthermore, we also find that if the outer sphere is kept motionless, the torque required to rotate the inner sphere increases almost linearly with the increase of n. This

information is of practical importance for the design of agitated polymeric reactors, for instance, among other potential engineering applications.

Notation

n power-law exponent of viscosity
P hydrodynamic pressure
r spherical coordinate
R radius of sphere
Re Reynolds number ($=\rho R_2^3\omega_S/\eta_0$)
t time
T torque
$\underline{V}$ velocity

Greek letters

η apparent viscosity
η_0 zero-shear-rate viscosity
$\dot{\gamma}$ magnitude of shear rate tensor
λ time constant for viscosity
ω angular velocity
Ω vorticity function
ϕ spherical coordinate
ψ stream function
ρ fluid density
θ spherical coordinate

Subscripts

1 inner sphere
2 outer sphere
s characteristic quantity

Superscripts

$*$ dimensionless quantity
T transpose of a matrix

Mathematical symbols

D^2 differential operator $\left(=\dfrac{\partial^2}{\partial r^2}+\dfrac{1}{r^2}\dfrac{\partial^2}{\partial\theta^2}-\dfrac{1}{r^2}\cot\theta\dfrac{\partial}{\partial\theta}\right)$
∇ gradient
∇^2 Laplacian ($=\nabla\cdot\nabla$)
$\cdot$ inner product

Underline

$\underline{\underline{\dot{\gamma}}}$ shear rate tensor
$\underline{V}$ velocity vector

Acknowledgements

This work is supported by the National Science Council of the Republic of China.

Appendix

The governing equations and the associated boundary conditions are solved numerically by a pseudo-spectral method (Gottlieb et al., 1984) based on Chebyshev polynomials. In this approach, an unknown function $f(r,\theta)$ is approximated by $f_{NM}(r,\theta)$, which is defined by

$$f_{NM}(r,\theta)=\sum_{i=0}^{N}\sum_{j=0}^{M} f_{NM}(r_i,\theta_j)\,g_i(r)g_j(\theta), \tag{A.1}$$

where $f_{NM}(r_i,\theta_j)$ is the value f_{NM} at the kth collocation point, $k=(N-1)i+j$. The interpolation polynomials $g_i(r)$ and $g_j(\theta)$ depend on the locations of the collocation points, which are determined by mapping the computational domain onto the region $[-1,1]\times[-1,1]$ by

$$r=\frac{R_2-R_1}{2}y+\frac{R_2+R_1}{2}, \tag{A.2}$$

$$\theta=\frac{\pi}{4}(x+1). \tag{A.3}$$

The $N+1$ interpolation points in the interval $[-1,1]$ are chosen to be the extreme values of an Nth-order Chebyshev polynomial ($T_N(y)$), $y_j=\cos(\pi j/N)$, $j=0,1,\ldots,N$, and the corresponding interpolation polynomial $g_j(y)$ is

$$g_j(y)=\frac{(-1)^{j+1}(1-y^2)\,(\mathrm{d}T_N(y)/\mathrm{d}y)}{c_jN^2(y-y_j)},$$
$$j=0,1,\ldots,N, \tag{A.4}$$

where $c_0=c_N=2$, and $c_j=1$, $1\leqslant j\leqslant N-1$. Partial derivatives $f_{NM}(r,\theta)$ are calculated by differentiating Eq. (A.1). The interpolation polynomials and the collocation points in the θ-direction are determined in a similar manner. The discretization scheme stated above leads to a set of non-linear algebraic equations for the stream function ψ and the vorticity function Ω, which is then solved by a Newton–Raphson iteration scheme. Double precision is used throughout the computation. Various mesh patterns were examined to assure that the mesh pattern is fine enough, and to guarantee the convergence of accuracy.

References

Bar-Yoseph, P.Z., Kryzhanovski, Yu., 1996. Axisymmetric vortex breakdown for generalized Newtonian fluid contained between rotating spheres. Journal of Non-Newtonian Fluid Mechanics 66, 145–168.

Bird, R.B., Armstrong, R.C., Hassager, O., 1977. Dynamics of Polymeric Liquids, Vol. 1, 2nd Edition, Wiley, New York.

Bird, R.B., Stewart, W.E., Lightfoot, E.N., 2002. Transport Phenomena, 2nd Edition. Wiley, New York.

Chu, J.W., Lin, W.S., Lee, E., Hsu, J.P., 2001. Electrophoresis of a sphere in spherical cavity at arbitrary electrical potentials. Langmuir 17, 6289–6297.

Dennis, S.C.R., Quartapelle, L., 1984. Finite difference solution to the flow between two rotating spheres. Computers and Fluids 12, 77–92.

Endo, Y., Kousaka, Y., 1996. Dispersion mechanism of coagulated particles in liquid flow. Colloids Surfaces A 109, 109–115.

Gottlieb, D., Hussaini, M.Y., Orszag, S.A., 1984. Spectral Methods for Partial Differential Equations. SIAM, Philadelphia, PA.

Greenspan, H.P., 1968. The Theory of Rotating Fluids. Cambridge University Press, New York.

Greenspan, D., 1975. Numerical studies of steady, viscous, incompressible flow between two rotating spheres. Computers and Fluids 3, 69–82.

Ide, Y., White, J.L., 1974. Rheological phenomena in polymerization reactors: rheological properties and flow patterns around agitators in polystrene–styrene solution. Journal of Applied Polymer Science 18, 2997–3018.

Karageorghis, A., 1991. A note on the satisfaction of the boundary conditions for Chebyshev collocation methods in rectangular domains. Journal of Scientific Computings 4, 21–26.

Lee, E., Chu, J.W., Hsu, J.P., 1998. Electrophoretic mobility of a sphere in a spherical cavity. Journal of Colloid Interface Science 205, 65–76.

Lee, E., Chu, J.W., Hsu, J.P., 1999. Electrophoretic mobility of a concentrated suspension of spherical particles. Journal of Colloid Interface Science 209, 240–246.

Lee, E., Yen, C.B., Hsu, J.P., 2000. Sedimentation of a non-conducting sphere in a spherical cavity. Journal of Physical Chemistry 104, 6815–6820.

Lee, E., Yen, F.Y., Hsu, J.P., 2001. Dynamic electrophoretic mobility of concentrated spherical dispersions. Journal of Physical Chemistry 105, 7239–7245.

Lee, E., Kao, J.D., Hsu, J.P., 2002a. Electrophoresis of a non-rigid entity in a spherical cavity. Journal of Physical Chemistry B 106, 8790–8795.

Lee, E., Lee, Y.H., Pai, Y.T., Hsu, J.P., 2002b. Flow of a viscoelastic shear-thining fluid between two concentric rotating spheres. Chemical Engineering Science 57, 507–514.

Lee, E., Huang, Y.F., Hsu, J.P., 2003. Electrophoresis in a non-Newtonian fluid: Sphere in a spherical cavity. Journal of Colloid Interface Science 258, 283–288.

Nakabayashi, K., Tsuchida, Y., 1995. Basic study on classification of fine particles in almost rigidly rotating flow (2nd report, dependence of Ekman layer and interior region on wall configuration of housing and rotor). Transactions of Japan Society of Mechanical Engineering, Part B 591 (61), 3996–4003.

Nakabayashi, K., Tsuchida, Y., Takeo, K., Ono, Y., 1995. Basic study on classification of fine particles in almost rigidly rotating flow (3rd report, conditions of occurrence of a stable regime of almost rigidly rotating flow). Transactions of the Japan Society for Mechanical Engineers, Part B 591 (61), 4004–4010.

Pearson, C.E., 1967. A numerical study of the time-dependent viscous flow between two rotating spheres. Journal of Fluid Mechanics 28, 323–336.

Pedlosky, J., 1969. Axially symmetric motion of a stratified, rotating fluid in a spherical annulus of a narrow gap. Journal of Fluid Mechanics 36, 401–415.

Schultz, D.H., Schwengels, S., Pralhad, R.N., Kocamustafaogullari, G., 1991. High-order method for heat transfer in a fluid between concentric rotating spheres. Computers and Fluids 20, 43–57.

Tucker III, C.L., 1989. Fundamentals of Computer Modeling for Polymer Processing. Hanser Publishers, Munich, Vienna, New York.